Modeling P-Loops Domain of Sodium Channel: Homology with Potassium Channels and Interaction with Ligands

Denis B. Tikhonov and Boris S. Zhorov
Department of Biochemistry and Biomedical Sciences, McMaster University, Hamilton, Ontario, Canada

ABSTRACT A large body of experimental data on Na^+ channels is available, but the interpretation of these data in structural terms is difficult in the absence of a high-resolution structure. Essentially different electrophysiological and pharmacological properties of Na^+ and K^+ channels and poor identity of their sequences obstruct homology modeling of Na^+ channels. In this work, we built the P-loops model of the Na^+ channel, in which the pore helices are arranged exactly as in the MthK bacterial K^+ channel. The conformation of the selectivity-filter region, which includes residues in positions −2 through +4 from the DEKA locus, was shaped around rigid molecules of saxitoxin and tetrodotoxin that are known to form multiple contacts with this region. Intensive Monte Carlo minimization that started from the MthK-like conformation produced practically identical saxitoxin- and tetrodotoxin-based models. The latter was tested to explain a wide range of experimental data that were not used at the model building stage. The docking of tetrodotoxin analogs unambiguously predicted their optimal orientation and the interaction energy that correlates with the experimental activity. The docking of μ-conotoxin produced a binding model consistent with experimentally known toxin-channel contacts. Monte Carlo-minimized energy profiles of tetramethylammonium pulled through the selectivity-filter region explain the paradoxical experimental data that this organic cation permeates via the DEAA but not the AAAA mutant of the DEKA locus. The model is also consistent with earlier proposed concepts on the Na^+ channel selectivity as well as Ca^{2+} selectivity of the EEEE mutant of the DEKA locus. Thus, the model integrates available experimental data on the Na^+ channel P-loops domain, and suggests that it is more similar to K^+ channels than was believed before.

INTRODUCTION

Voltage-gated Na^+ channels belong to the superfamily of P-loop channels, which includes K^+ and Ca^{2+} channels as well as channels gated by cyclic nucleotides and glutamate (see Zhorov and Tikhonov, 2004). The channels are formed by four membrane-spanning domains arranged around the central pore. The pore-forming region of each domain includes the transmembrane outer helix *S5*, the membrane reentrant P-loop, and the transmembrane inner helix *S6*. The x-ray structures of several bacterial K^+ channels in the closed and open states (Doyle et al., 1998; Jiang et al., 2002, 2003; Kuo et al., 2003) show that each P-loop folds up to form five segments:

1. The N-terminal extracellular linker following the outer helix.
2. The pore helix.
3. A short turn exposed to the large water-lake cavity inside the pore.
4. The pore-facing selectivity-filter region.
5. The linker between the selectivity-filter region and the inner helix.

The pore helices, the turn, and the selectivity-filter region have similar three-dimensional structures in the closed and open K^+ channels. The extracellular parts of the inner and outer helices that form close contacts with the pore helices are also similar in both the open and closed K^+ channels. In the absence of x-ray structures of other P-loop channels, homology with K^+ channels is employed in attempts to understand their structure-function relationships.

The pore-forming α_1-subunit of Na^+ channels has four nonidentical repeats within a single polypeptide chain. Each repeat incorporates the S_1–S_4 domain with the voltage sensor and the pore domain S_5-*P*-S_6. In K^+ channels, the selectivity filter is formed by the backbone oxygens from the signature sequence *TXGYG* (Doyle et al., 1998). In the Na^+ channel, highly conserved residues Asp, Glu, Lys, and Ala, in repeats I–IV, respectively form a ring called the *DEKA locus*. The side chains of the DEKA locus govern selective permeability of Na^+ channels (Heinemann et al., 1992).

In all P-loop channels, residues governing selectivity are located near the C-termini of the pore helices. Since P-loop channels differ greatly in ion selectivity, it is expected that the structural details of their selectivity filters are very specific. In K^+ channels, the conserved *TXGYG* motif forms a narrow tunnel, in which ions are coordinated by the main chain carbonyls. This three-dimensional structure is stabilized by inter- and intrasegment H-bonds (Doyle et al., 1998). Selectivity filters of other channels have been modeled. Models for glutamate-gated channels integrate data on the pore dimensions, activity of channel blocking drugs, and mutational analysis (Tikhonov et al., 1999, 2002). Models of the Na^+

Submitted June 23, 2004, and accepted for publication October 1, 2004.

Address reprint requests to Dr. Boris Zhorov, Dept. of Biochemistry and Biomedical Sciences, McMaster University, 1200 Main Street West, Hamilton, Ontario, L8N 3Z5 Canada. Tel.: 905-525-9140 ext. 22049; Fax: 905-522-9033; E-mail: zhorov@mcmaster.ca.

Denis B. Tikhonov is on leave from the Sechenov Institute of Evolutionary Physiology and Biochemistry, St. Petersburg, Russia.

0006-3495/05/01/184/14 $2.00

doi: 10.1529/biophysj.104.048173

channel were proposed to explain experimental data on mutations and blockade by guanidinium toxins (Lipkind and Fozzard, 2000; Khan et al., 2002). Diverse models of the L-type Ca^{2+} channel were elaborated (Zhorov et al., 2001; Lipkind and Fozzard, 2001). All these models use x-ray structures of K^+ channels as templates for general folding. However, the selectivity filters that control specific properties of K^+, Na^+, and Ca^{2+} channels should have different structures. For instance, in K^+ channels, the permeating cations interact with the backbone carbonyl groups in the selectivity-filter region, whereas in other P-loop channels the permeating ions are believed to interact with the side chains of selectivity-filter residues. In the models of the Na^+ channel (Lipkind and Fozzard, 2000) and glutamate-gated channels (Tikhonov et al., 2002) the pore helices were placed more distant from the pore axis than in K^+ channels to make a wider channel. In the Na^+ channel model (Lipkind and Fozzard, 2000), the wider channel provides access of tetrodotoxin (TTX) and saxitoxin (STX) to the selectivity-filter residues. Furthermore, the wider pore at the level of the selectivity filter could explain the fact that organic cations, which do not permeate via K^+ channels, permeate via other P-loop channels (Burnashev et al., 1996; Hille, 1971, 1973; McCleskey and Almers, 1985).

There is a major problem with moving the pore helices from the pore axis. The pore helices form close contacts with the inner and outer helices. To preserve these contacts, the latter segments should be also moved. This relocation would affect folding of the entire channel. To avoid this, Zhorov et al. (2001) created a model of the L-type Ca^{2+} channel in which all the helices occupied the same positions as in KcsA. The wider pore at the selectivity-filter level was achieved by Monte Carlo minimizations of four hexapeptide segments (one from each repeat) around the selectivity-filter residues whose side chains were constrained to Ca^{2+} ions. The obtained structure did not have bad contacts, demonstrating that significant rearrangement of the selectivity-filter region is possible without disrupting the disposition of the pore helices.

The problem of the x-ray template flexibility is generally important for homology modeling of proteins. Obviously, the geometry of flexible loops, and the disposition of mobile domains and segments connected by hinges, can differ between homologous proteins. Can homologous proteins sharing the same fold differ significantly in the area of densely packed domains? This question is particularly important for studies of P-loop channels that employ high-resolution structures of bacterial K^+ channels as templates. One of the goals of this work was to investigate whether experimentally available data on the Na^+ channel selectivity-filter region can be explained without major modification of the x-ray template of the P-loop region. The selectivity filter of the Na^+ channel is particularly suitable for such studies because a large body of experimental data is available. It is well known that Na^+ selectivity is controlled by the DEKA locus. In Ca^{2+} channels, ion selectivity and permeation are controlled by the EEEE locus formed by four glutamates, which occupy positions homologous to the DEKA locus in Na^+ channels (Kim et al., 1993; Yang et al., 1993). The replacement of the DEKA locus by four glutamates renders a Ca^{2+}-selectivity to the channel (Heinemann et al., 1992; Favre et al., 1996).

Data on the Na^+ channel blockade by guanidinium toxins provide unique possibilities to design and test molecular models. Tetrodotoxin (TTX) and saxitoxin (STX) block the voltage-gated Na^+ channel in nanomolar concentrations (Narahashi et al., 1967). These toxins interact with residues in the DEKA locus and downstream from it (Noda et al., 1989; Terlau et al., 1991; Kirsch et al., 1994; Penzotti et al., 2001; Choudhary et al., 2003). The structure-activity relationships of TTX derivatives (Kao and Walker, 1982; Kao, 1986; Yotsu-Yamashita et al., 1999) revealed the importance of specific groups, thus providing additional information to be explained. TTX, STX, and their derivatives have a generally similar mechanism of action, but some residues of the Na^+ channel interact differently with individual toxins (Satin et al., 1992; Penzotti et al., 1998).

Peptide toxins known as μ-conotoxins (Olivera et al., 1990) represent another class of ligands that act on the Na^+ channel by the channel-blocking mechanism (Cruz et al., 1985; Ohizumi et al., 1986). The toxins have a critical arginine that could mimic the guanidinium group of TTX and STX (Yanagawa et al., 1987; Sato et al., 1991; Becker et al., 1992; Dudley et al., 1995; Chahine et al., 1995). However, mutations eliminating the sensitivity to TTX and STX are less critical for conotoxins (Chahine et al., 1998; Stephan et al., 1994; Li et al., 1997), indicating that residues beyond the TTX receptor are involved in the interaction with the large conotoxin peptide. The critical arginine residue of μ-conotoxin is likely to bind to the outer ring of negatively charged residues (Chang et al., 1998; Hui et al., 2002).

The above experimental data were integrated in models visualizing toxins bound to the selectivity filter and outer vestibule of the Na^+ channel (Lipkind and Fozzard, 2000; Choudhary et al., 2003). The general pattern of interactions between specific functional groups of toxins and individual amino acids is well documented and presently does not need to be revised. However, the above models are descriptive rather than numerical. The ability of these models to sustain the above pattern of ligand-receptor contacts in molecular dynamics or Monte Carlo calculations has not been demonstrated. Independent testing of the models is not possible, because atomic coordinates are not available.

In this work we built a model of the Na^+ channel P-loops region assuming its strong structural similarity with K^+ channels by the disposition of the pore helices. We applied the Monte Carlo minimization protocol to search the energetically optimal position and orientation of the ligands in the selectivity-filter region. The optimal complexes found are in exact agreement with the general scheme of specific ligand-receptor interactions. The predicted binding energy of the TTX analogs quantitatively correlates with the experimental

activity. The model is consistent with numerous experimental data that were not used at the model building stage, including mutational analysis, permeation of organic ions, and ion selectivity.

METHODS

The amino acid sequence corresponds to the $Na_v1.4$ channel from rat skeletal muscle. The model consists of N-terminal parts of P-loops from four repeats (Table 1). Each repeat includes the pore helix, a turn, the selectivity-filter region, and a short segment following the selectivity-filter region. The x-ray structure of the MthK bacterial K^+ channel (Jiang et al., 2002) was used as a template for homology modeling. The sequence alignment between MthK, Na^+, and Ca^{2+} channels is shown in Table 1. This alignment was used in studies of Ca^{2+} channels (Zhorov et al., 2001; Yamaguchi et al., 2003) and Na^+ channels (Yamagishi et al., 2001). Large extracellular linkers between the selectivity filter and the inner pore were not included in the model because the crystallographic structure of this part is not available. When viewed from the extracellular surface, the repeats I–IV were arranged in a clockwise fashion around the central pore (Dudley et al., 2000). The four repeats were not linked to each other.

The conformational energy expression included van der Waals, electrostatic, solvation, and torsion components. Nonbonded interactions were calculated using the AMBER force field (Weiner et al., 1984). Electrostatic interactions were calculated with a distance-dependent dielectric ($\varepsilon = r$). All ionizable groups in the protein, ligands, and peptide toxins were modeled in the ionized form. Nonbonded interactions were truncated at distances >8 Å. The cutoff was not applied to electrostatic interactions involving ionized groups; these interactions were computed at all distances. The hydration energy was calculated by the implicit-solvent method (Lazaridis and Karplus, 1999).

All-*trans* starting conformations were assigned for side chains of those residues that are different between MthK and the Na^+ channel. The N- and C-termini of the P-loop fragments were constrained to positions seen in the MthK x-ray structure. Four residues in each repeat, including residues in the DEKA locus and three positions downstream, were treated as completely flexible. The α-carbons of other residues were constrained to corresponding positions in the MthK template with the help of pins. A pin is a flat-bottom penalty function (Brooks et al., 1985) that allows penalty-free deviations of the respective atom up to 1 Å from the template and imposes an energy penalty for larger deviations. Flat-bottom constraints were also used to impose experimentally known ligand-receptor contacts.

The optimal conformations were searched by the Monte Carlo minimization (MCM) protocol (Li and Scheraga, 1987). Energy was minimized in the space of generalized coordinates using the ZMM program (Zhorov, 1981). MC-minimizations were terminated when the last 2000 energy minimizations did not improve the energy of the best minimum found. All MC-minimizations were performed in two stages. In the first stage, the energy was MC-minimized with pins and ligand-receptor constraints. After the constrained MCM trajectory converged, all constraints were removed and the model was refined by the unconstrained MCM trajectory. The difference between structures found in the constrained and unconstrained trajectories indicated whether the constrained search yielded a stable structure or a conformation with bad contacts. Other details of the MCM protocol implementation in the ZMM program are described elsewhere (Zhorov and Ananthanarayanan, 1996; Zhorov and Lin, 2000).

The ligands were built and their geometry was optimized using the ZMM program. All torsional and bond angles of ligands were treated as variables. The atomic charges of ligands were calculated by the AM1 method (Dewar et al., 1985) using the MOPAC program. Peptide toxins were built using structural information available from their nuclear magnetic resonance studies (Wakamatsu et al., 1992). The geometry of toxins was MC-minimized.

MC-minimized energy profiles of drugs pulled via the pore were computed as described elsewhere (Zhorov and Lin, 2000; Zhorov and Bregestovski, 2000). The plots of MC-minimized energy against the toxins' orientation in the selectivity filter were computed by constraining the dihedral angle between the plane comprising the pore axis and another plane passing through the long axis of the ligand. The latter was drawn from the central carbon atom in the guanidinium group to a carbon atom at the opposite side of the drug. The dihedral constraint freezes one of the six rigid-body degrees of freedom of the ligand. The constrained dihedral angle was increased with a 15° step. At each step the energy was MC-minimized with all other degrees of freedom being allowed to vary.

RESULTS

Building the P-loop model and searching the optimal binding mode of TTX and STX

The underlying idea in the present modeling was to preserve the general folding of the P-loop region as seen in K^+ channels and to rearrange only residues in the selectivity-filter region. To do this, we employed the fact that the rigid molecules, TTX and STX, form multiple well-defined contacts with several residues in the selectivity-filter region. In other words, the idea was to shape the flexible selectivity-filter region around the toxins with biasing these contacts. We have built two independent models by shaping the flexible segments of the protein around TTX and STX.

The following interactions were used as constraints to build the *TTX-based model*:

1. The guanidinium group of TTX binds to Asp^{400} in repeat I and Glu^{755} in repeat II.

TABLE 1 Aligned sequences of P-loops in K^+, Na^+, Ca^{2+}, and GluR channels

Type	Channel	Domain	First residue	
K^+	KcsA		59	LITYPRAL WWSVETATTV GYGDLY
	MthK		43	GESWTVSL YWTFVTIATV GYGDYS
Na^+	$Na_v1.4$	I	383	YDTFSWAF LALF**R**LMTQ**D** **YWE**NLF
		II	738	MNDFFHSF LIVFRILCG**E** **W**I**E**TMF
		III	1220	YDNVGLGY LSLLQVATF**K** **GWMD**IM
		IV	1512	FETFGNSI ICLFEITTS**A** G**WD**GLL
Ca^{2+}	$Ca_v1.2$	I	376	FDNFAFAM LTVFQCITME GWTDVL
		II	719	FDNFPQSL LTVFQILTGE DWNSVM
		III	1128	FDNVLAAM MALFTVSTFE GWPELL
		IV	1429	FQTFPQAV LLLFRCATGE AWQDIM

TTX and STX-sensing residues revealed in mutational experiments (see Introduction) are underlined. Residues that contribute >1 kcal/mol to the interaction energy with TTX are in boldface type.

2. Hydroxyls 9 and 10 of TTX interact with Glu^{758} in repeat II.
3. The hydrophobic side of TTX interacts with Tyr^{401}.

The following interactions were used as constraints to build the *STX-based model*:

1. The 7,8,9 guanidinium group interacts with Asp^{400} in repeat I and with Glu^{755} in repeat II.
2. The 1,2,3-guanidinium group interacts with Glu^{1532} in repeat IV.
3. Hydroxyl 12 interacts with Glu^{758} in repeat II.

The experimental data that justify these constraints are summarized by Lipkind and Fozzard (2000) and Choudhary et al. (2003).

All bad contacts unavoidable in the MthK-based starting conformation were eliminated during MC-minimizations of both models. Importantly, no conflicts occurred between the ligand-receptor constraints and pin constraints in P-loops and residues following the selectivity-filter region. This indicates that the MthK-based model has enough space to accommodate TTX and STX without displacing the pore helices.

TTX and STX receptors have two rings with acidic residues. The guanidinium group of TTX and 7,8,9 guanidinium group of STX are known to bind to the DEKA locus. The opposite ends of the ligands have multiple donors of protons that bind to the outer ring of acidic residues containing Glu^{403}, Glu^{758}, and Asp^{1532}. Obviously, various orientations of the toxins are possible, in which their multiple functional groups form H-bonds with the outer ring of the acidic residues. To explore whether the ligand orientation imposed by the experimental constraints is energetically optimal, we computed a MC-minimized energy profile for the ligand rotated around its long axis. At each point of the profile, one angle defining the ligand orientation was constrained, but all other degrees of freedom were allowed to vary in the MC-minimization (see Methods). In this stage, we did not impose any constraints biasing ligand-receptor interactions. The rotational profiles for both TTX and STX have a single well-shaped minimum (Fig. 1) at the orientations that correspond to the MC-minimized structures shaped around the ligands (see above). This result shows that energetically preferable orientations of TTX and STX do not depend on their initial placement.

The independently built TTX-based and STX-based models are nearly identical in terms of geometry of the toxin binding sites (Fig. 2). The RMSD of all heavy atoms between the two models is 0.73 Å. The RMSD of heavy atoms in the toxin binding site is 0.41 Å. The RMSD of α-carbons in this region is as small as 0.29 Å. The obtained similarity between the independently built models is not trivial because toxins are different in structure. The similarity justifies our model-building approach. Since the TTX-based and STX-based models are practically similar, we describe below only the model shaped around TTX.

In the selectivity-filter region, large side chains of Trp^{402}, Trp^{756}, Ile^{757}, Trp^{1239}, and Trp^{1531} face the interfaces between

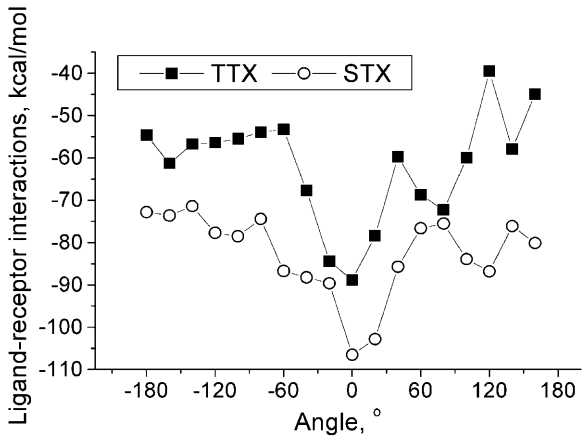

FIGURE 1 Ligand-receptor energy obtained from the MC-minimized energy profiles of TTX and STX rotated in the channel. The zero angles correspond to the energetically optimal orientations shown in Fig. 4. Positive values correspond to the anticlockwise rotation when viewed from the extracellular side. The unimodal character of the energy profiles indicates unambiguously the preferable orientation of the toxins in the channel. The minima are 40–60° in width, indicating a certain flexibility of the complexes, which is due to the long side chains of the protein that follow the rotated ligand.

the pore helices. Interestingly, the large residues approach the α-carbons of Gly^{1238} and Gly^{1530}, making knob-into-the-hole contacts. Some of these residues were reported to affect the ion permeation through Na^+ channels (Tsushima et al., 1997). Tyr^{401} forms an H-bond with Glu^{403}. As a result, the aromatic ring of Tyr^{401}, a residue important for TTX binding, faces the pore and can interact with toxins. The arrangement of large residues around Gly^{1530} is shown in Fig. 2 *B*. In our model, Arg^{395} forms a salt bridge with Asp^{400}, but does not impede interactions of Asp^{400} with TTX and STX. Specifically interacting partners were not found for Arg^{750}.

At first sight, the fact that bulky guanidinium toxins bind to the Na^+ channel selectivity filter suggests that its structure should significantly diverge from the narrow K^+ channels. However, our models have rather small backbone deviations from MthK only in a limited region around the selectivity filter. These deviations provide enough space for the binding of toxins (Fig. 3). The narrowness of the K^+ channel selectivity filter does not mean the lack of space in the P-loops region. Indeed, the pore-lining backbones are distant from pore helices due to H-bonds between large chains, including intrasubunit H-bonds $Trp^{67}\cdots Asp^{80}$ and intersubunit H-bonds $Trp^{68}\cdots Tyr^{78}$ (KcsA numbering, see Table 1). Notably, these pairs of H-bonding residues are absent in the sequences of Na^+ channels. This allows more compact packing of the selectivity-filter region against the pore helices, thus providing more space in the Na^+ channel outer vestibule.

Interactions of TTX and STX with the model

Complexes of STX and TTX with the Na^+ channel are shown in Fig. 4. The number of ligand-receptor constraints used to build the model (see above) is much smaller than the number

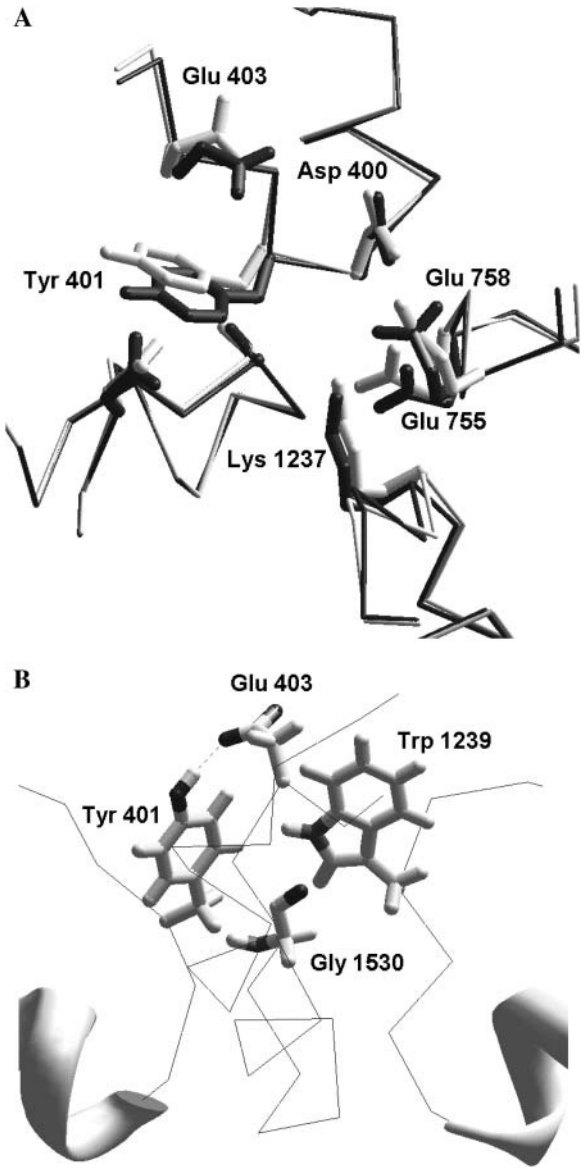

FIGURE 2 The model of the selectivity-filter region. (*A*) The top view of the superposition of models shaped around TTX (*black*) and STX (*gray*). Both models are practically identical in terms of backbone folding and side-chain geometry in the toxin binding sites. Sticks represent residues in the DEKA locus, Tyr^{401}, and the outer ring of acidic residues (Glu^{403}, Glu^{758}, and Asp^{1532}). (*B*) The side view showing the arrangement of large residues around Gly^{1530}. For clarity, only two pore helices are shown as ribbons. Tyr^{401}, the residue important for TTX binding (Backx et al., 1992), forms an H-bond with Glu^{403} and exposes the aromatic ring to the pore where it can interact with toxins.

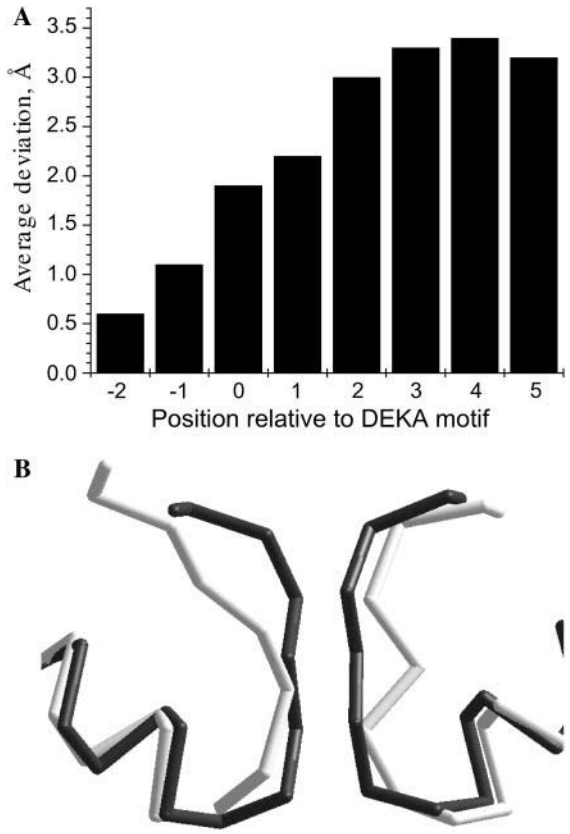

FIGURE 3 The comparison of the Na^+ channel model with the MthK template. (*A*) Deviations of α-carbons from the template (averaged over four repeats). (*B*) The α-carbon tracings of MthK (*black*) and Na^+ channel (*gray*). Only repeats I and III are shown for clarity.

of specific ligand-receptor contacts found in the MC-minimized complexes. Many of these contacts were observed in experiments (see Table 1). Thus, the hydrophobic side of TTX interacts with the aromatic ring of Tyr^{401} in agreement with the data that this residue determines the TTX sensitivity of the Na^+ channel (Backx et al., 1992). The hydrophobic side of STX binds to the hydrophobic Met^{1240} side chain. The energy components of the ligand-receptor complexes are shown in Table 2. Solvation and van der Waals interactions provide significant contributions to the ligand-receptor energy. However, these interactions are similar for TTX and STX and weakly depend on their orientation. The reason is that the toxins have a conical shape, which is complimentary to the channel conical vestibule. Therefore, the contact surfaces between the toxins and receptor are similar, and similar amounts of water molecules are displaced upon the binding of both toxins. Electrostatic interactions provide the largest contribution to the ligand-receptor energy. This is not surprising, taking into account that the ligand and the receptor have oppositely charged groups. The charge complementarity with the receptor is the major determinant of the toxins' orientation. The largest contributions to the ligand-receptor energy are provided by aspartates and glutamates in the selectivity filter and carboxyl residues in the outer ring (Table 3). It should be noted that the absolute values of the electrostatic energy are obviously overestimated because solvent counterions were not taken into account.

Binding of TTX derivatives

A touchstone for any homology model is its ability to bind drugs that were not used at the stage of model building. There

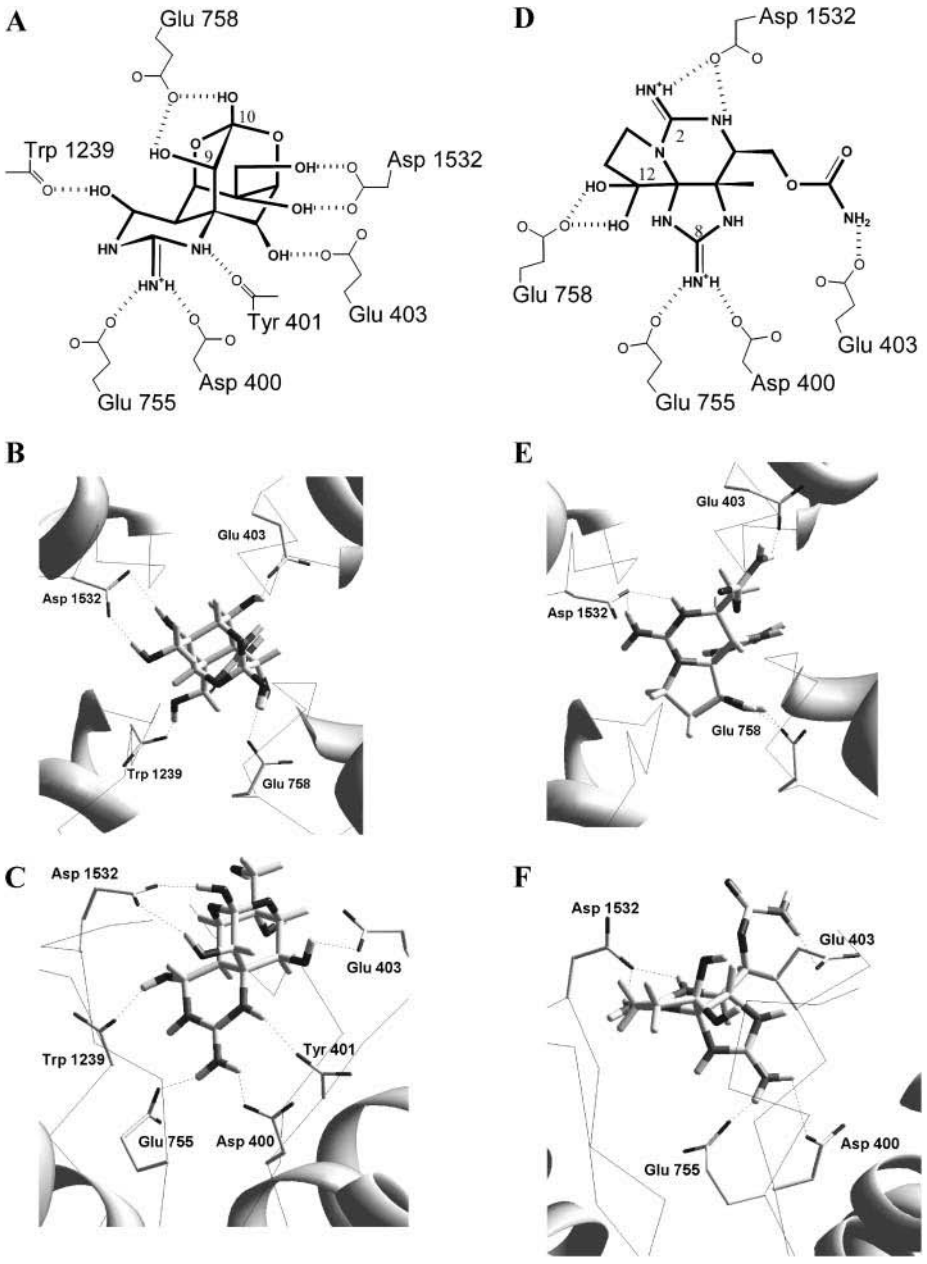

FIGURE 4 The binding of TTX (*A–C*) and STX (*D–F*) in the Na^+ channel model. (*A* and *D*) Specific contacts of TTX and STX with residues in the selectivity-filter region predicted in our models. (*B* and *E*) Extracellular views of the complexes. P-loops are shown as ribbons and the backbones in the selectivity-filter region as α-carbon tracings. (*C* and *F*) Side views of the complexes. Ligand-receptor H-bonds are shown.

are many analogs of TTX and STX, whose activity varies in a broad range (see e.g., Yotsu-Yamashita et al., 1999). To test our model, we have selected four representative derivatives (Fig. 5 *A*) using the following criteria. First, we did not include compounds for which the lack of activity was obviously deducible from their structure. Second, the compounds selected have essentially different structures. Third, the activity of the selected compounds varies in a broad range, from nM to μM (Table 4). We did not make any adjustments of the model to dock the TTX analogs. For each analog, a rotational energy profile was calculated (Fig. 5 *B*). As in the case of TTX and STX, each profile has a well-defined minimum, which predicts unambiguously the optimal orientation of the ligand in the channel. As in the case of TTX and STX, the optimal orientation and the binding energy was mainly determined by the electrostatic complementarity of the ligands with acidic residues in the DEKA locus and in the outer ring. Notably, our calculations revealed a strong correlation between the experimentally observed activity and predicted binding energy (Table 4). Thus, our model allows quantitative analysis of the structure-activity relationships of guanidinium toxins.

Binding of μ-conotoxin

Peptide toxins dramatically differ in structure from TTX and STX. Therefore, the model's ability to explain known aspects of the peptide toxins' action may serve as an additional

TABLE 2 Energy characteristics of optimal complexes of TTX and STX with Na^+ channel

	Ligand-receptor energy and its components, kcal/mol				
Compound	Total	Electrostatic	van der Waals	H-bonds	Solvation
TTX	−93.7	−102.4	−21.2	−3.1	32.9
STX	−106.5	−115.4	−19.7	−2.1	30.7

important criterion of the model's validity. Since peptide toxins are much larger than TTX and STX, many residues in the outer vestibule are known to affect the binding of conotoxins. Experimental data indicate that Arg^{13} of μ-conotoxin interacts more strongly with the outer carboxylic ring than with the DEKA locus. Visual inspection of our model does not rule out the possibility that the guanidinium group of Arg^{13} in μ-conotoxin could reach the DEKA locus and interact with it as do TTX and STX. Another positively charged residue of μ-conotoxin, Lys^{16}, is also known to interact with the channel, but the interacting partners are uncertain. According to Dudley et al. (2000), the most probable partner is Asp^{1532} (repeat IV), whereas Li et al. (2001) revealed a strong interaction of Lys^{16} with Asp^{1241} (repeat III).

To explore these possibilities, we MC-minimized the nuclear magnetic resonance structure of the toxin (Wakamatsu et al., 1992; PDB code: 1TCG) and manually docked it in the orientation suggested by Dudley et al. (2000), who defined the interaction patterns between μ-conotoxin specific residues and the channel repeats. Then this interaction pattern was used as a constraint in a two-stage MCM docking. The unconstrained search did not significantly change the binding modes of the toxin that were imposed in the constrained search. More importantly, the conotoxin-based model did not deviate significantly from the TTX/STX-based model. The

TABLE 3 Energy contributions (kcal/mol) of P-loop residues to binding of TTX and STX

TTX		STX	
Residue	Energy	Residue	Energy
Glu^{755}	−23.1	Asp^{1532}	−28.7
Asp^{400}	−16.8	Glu^{758}	−21.8
Glu^{758}	−15.4	Glu^{755}	−21.8
Glu^{403}	−15.2	Asp^{400}	−21.8
Asp^{1532}	−13.5	Glu^{403}	−8.1
Trp^{1239}	−6.8	Arg^{395}	10.1
Tyr^{401}	−7.0	Tyr^{401}	−5.2
Lys^{1237}	7.7	Trp^{1239}	−1.1
Arg^{395}	7.1	Lys^{1237}	6.4
Trp^{756}	−2.1	Trp^{756}	−2.5
Met^{1240}	−1.8	Trp^{1531}	−3.1
Gly^{1238}	−1.2	Trp^{402}	−1.7
Trp^{402}	−1.1	Met^{1240}	−1.1
Trp^{1531}	−1.1	Glu^{1241}	−1.1
Ala^{1529}	−1.0	Ala^{1529}	−1.1

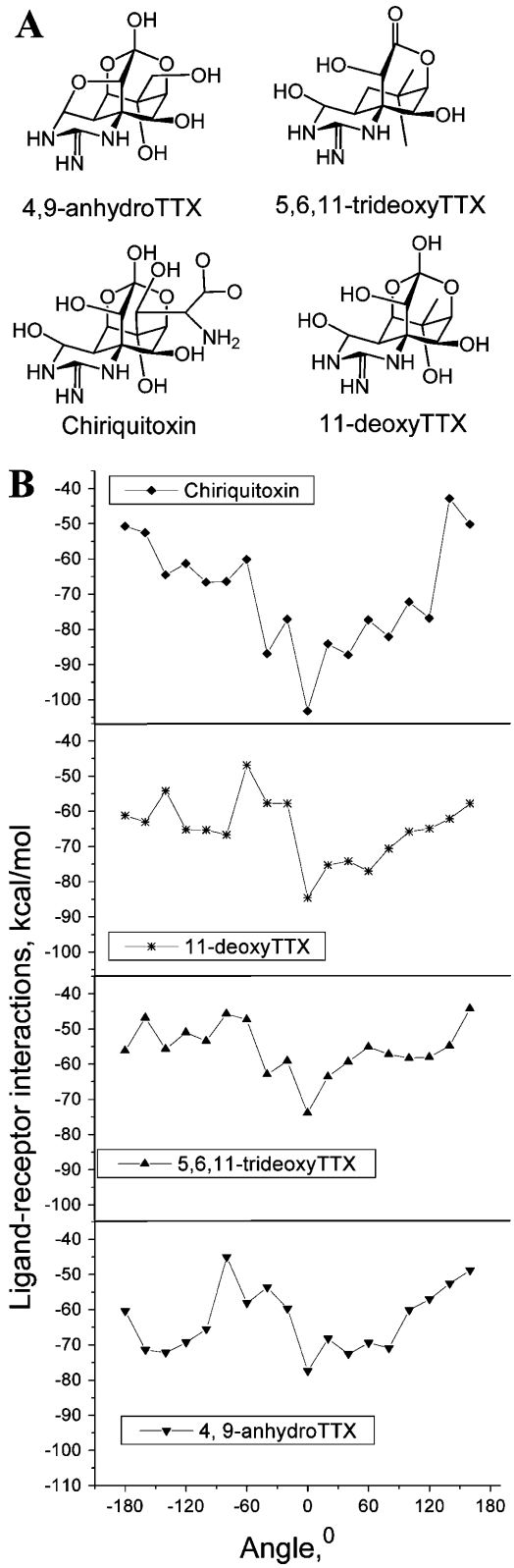

FIGURE 5 The binding of TTX derivatives. (*A*) Chemical structures. (*B*) Ligand-receptor energy obtained from the profiles of MC-minimized energy of the ligands rotated in the selectivity filter. The profiles are normalized to have the lowest minimum at zero angle. Each profile has a single energy minimum that predicts the optimal orientation of the molecule.

TABLE 4 Experimental activity (Yotsu-Yamashita et al., 1999) and calculated binding energy of TTX and its derivatives

Compound	Activity, nM	Binding energy E, kcal/mol	ΔE,* kcal/mol
Chiriquitoxin	1.0	−103.2	−29.3
TTX	1.8	−93.7	−19.8
11-deoxyTTX	37	−84.6	−10.7
4,9-anhydroTTX	180	−77.4	−3.5
5,6,11-trideoxyTTX	>5000	−73.9	0

*Relative to the weakest ligand 5,6,11-trideoxyTTX. The absolute values of the binding energy are overestimated because counterions are not included in the model.

RMSD of the main-chain atoms was 0.54 Å for the region upstream of the DEKA locus and 0.59 Å for the selectivity-filter region (between the DEKA and the outer ring of acidic residues). When 24 superficial residues in six positions downstream from the DEKA locus were taken into account, the RMSD between the TTX/STX- and conotoxin-based models increased to 1.67 Å. This is not surprising since the superficial residues do not significantly contribute to the TTX/STX binding but some of them (Asn^{404}, Thr^{759}, and Asp^{1241}) were constrained to μ-conotoxin.

The binding of the conotoxin molecule is shown in Fig. 6. In the compact outer vestibule, the large guanidinium group of Arg^{13} can interact with Glu^{758} and simultaneously approach the DEKA locus. The side chain of Lys^{16} is projected toward the interface between repeats III and IV. The close disposition of the channel repeats allows the amino group of Lys^{16} to make a bridge between Asp^{1241} and Asp^{1532}. Partitioned interaction energies for these two residues are shown in Table 5. It should be noted that both residues have more than one significantly interacting partner. The energies of specific interactions are in a qualitative agreement with experimental data (Chang et al., 1998; Dudley et al., 2000; Li et al., 2001).

Permeability for organic cations

Native Na^+ channels are not permeable for organic cations larger than guanidine (Hille, 1971). The probable reason is the strong electrostatic and H-bonding contacts between the DEKA side chains, which converge at the pore axis. However, strong transmembrane voltage results in a detectable permeability for large organic cations (Huang et al., 2000). The substitution of the DEKA lysine by alanine can break the inter-residue contacts and cause the channel to become less selective and permeable to cations as large as tetramethylammonium (TMA) and tetraethylammonium (Sun et al., 1997). However, the mutants do not behave as a simple molecular sieve because, paradoxically, the AAAA mutant of the DEKA locus is not permeable to TMA (Sun et al., 1997). The permeability to organic cations may be a critical test for our model, which is based on the K^+ channel structure and therefore has a seemingly narrower pore lumen than previous models.

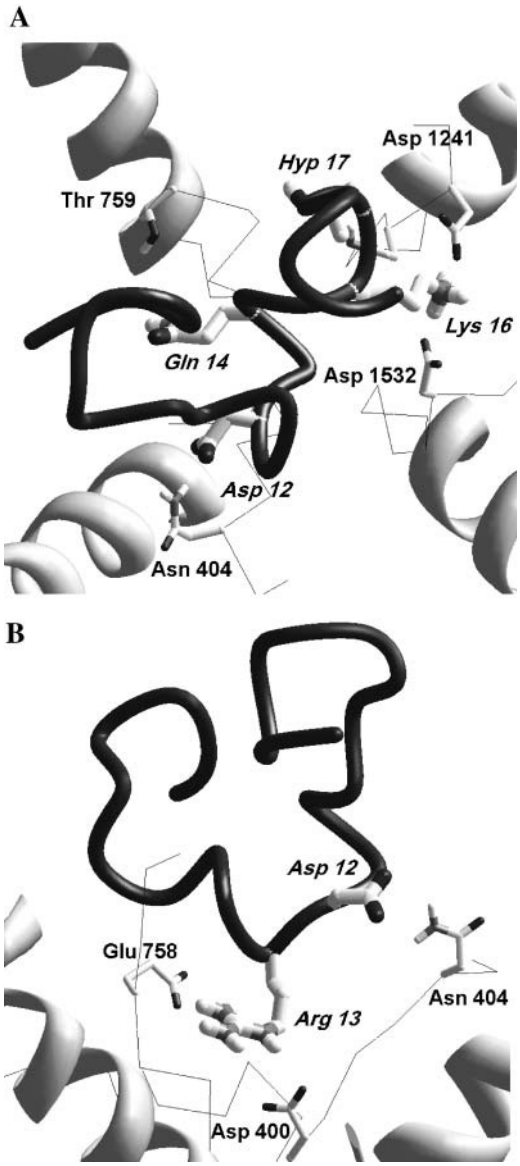

FIGURE 6 The binding of μ-conotoxin to the Na^+ channel model. (*A* and *B*) Top and side views at the complex. The toxin backbone is dark-shaded; pore helices of the channel are shown as white ribbons and backbones in the selectivity-filter region as α-carbon tracings. The side chains of specifically interacting residues are shown as sticks. The toxin residues are thick and the channel residues are thin.

To test whether the above experiments conflict with our model, we replaced the DEKA locus with AAAA and DEAA residues, constrained the TMA nitrogen to a plane normal to the pore axis, and computed 30 MCM trajectories by progressively shifting the constraining plane along the pore axis with a 1 Å step. The MC-minimized energy profiles (Fig. 7) have negative energies, clearly indicating the absence of critical sterical obstacles for TMA passing through the selectivity filter. The TMA energy in the AAAA mutant has two minima separated by a barrier. The first minimum corresponds to the electrostatic interaction with the external

TABLE 5 Energy contributions (kcal/mol) of P-loop residues to binding of Arg^{13} and Lys^{16} of μ-conotoxin

Arg^{13}		Lys^{16}	
Residue	Energy	Residue	Energy
Glu^{758}	−32.23	Asp^{1532}	−32.85
Asp^{400}	−10.49	Asp^{1241}	−32.57
Glu^{403}	−8.25	Glu^{758}	−7.42
Lys^{1237}	6.45	Ser^{1535}	−4.07
Glu^{755}	−5.62	Glu^{403}	−3.10
Asp^{1532}	−4.80	Lys^{1237}	2.90
Arg^{395}	4.75	Glu^{755}	−2.31
Tyr^{401}	−4.33	Glu^{1524}	−1.74
Arg^{750}	3.37	Asp^{400}	−1.64
Asp^{1241}	−3.36		
Trp^{756}	−3.04		
Glu^{1524}	−2.51		
Trp^{402}	−2.44		

ring of acidic residues. The second minimum occurs close to the focus of four helical macrodipoles. The TMA permeation would be obstructed by the barrier, which is caused by unfavorable electrostatic interactions of TMA in the vicinity of the AAAA locus. The barrier disappears in the DEAA locus, whose flexible acidic residues attract TMA without imposing the steric hindrances. The outer ring of the acidic residues and the DEAA locus form a nucleophilic tunnel from the outer vestibule to the inner pore.

Selectivity

Any model of the P-loop region should explain the major experiments addressing its ion selectivity. A quantitative analysis of permeation of inorganic cations requires extensive MD and free energy calculation. This is a challenging job even for K^+ channels with determined x-ray structures (Aqvist and Luzhkov, 2000; Berneche and Roux, 2001; Shrivastava et al., 2002). Our model is not precise enough for such simulations, but it allows a qualitative analysis of structural determinants of selectivity. The Na^+ channel selectivity-filter model (Lipkind and Fozzard, 2000) suggests that a water molecule is stabilized by H-bonds with the DEKA aspartate and lysine, whereas the DEKA lysine and glutamate form a salt bridge. An approaching Na^+ ion would displace the water molecule and bind between the aspartate and glutamate, whereas lysine would move toward the DEKA alanine to provide room for Na^+. To test the agreement between our model and this hypothesis, we placed a water molecule in the DEKA locus and imposed the above contacts by constraints. The two-stage MC-minimization demonstrated that the arrangement of the water molecule and DEKA residues is easily reproducible in our model and does not change after removing the constraints (Fig. 8). Numerous mutations in the DEKA locus are known to affect ion selectivity. The consistency of our model with the hypothesis of Lipkind and Fozzard (2000) implies similar explanations of how the mutations would affect the channel selectivity.

The conversion of Na^+ selectivity to Ca^{2+} selectivity by replacing the DEKA locus with the EEEE locus (Heinemann et al., 1992; Favre et al., 1996) deserves special mention, because these data are related to the problem of the three-dimensional similarity among K^+, Na^+, and Ca^{2+} channels. Structural models of the Ca^{2+} selectivity filter (Lipkind and Fozzard, 2001; Zhorov et al., 2001) propose that four glutamates in the EEEE locus bind two Ca^{2+}. Lipkind and Fozzard (2001) proposed that the side chains of four glutamates converge to form a narrow ring; two Ca^{2+} ions bind at the top and bottom faces of the ring and permeate in a single-file mode. An alternative model suggests that at millimolar Ca^{2+} four glutamates split in two pairs, each

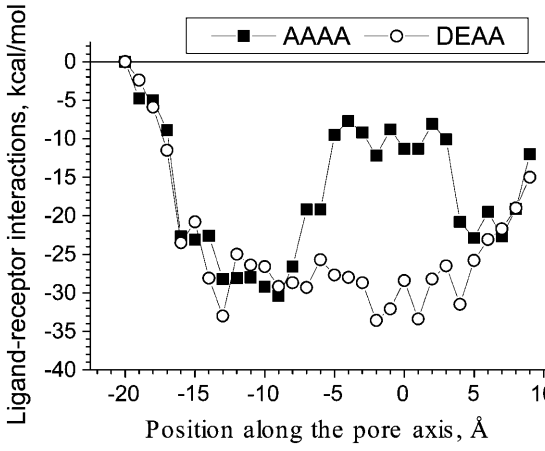

FIGURE 7 The ligand-receptor energy obtained from the profiles of MC-minimized energy of TMA pulled through the channel mutants in which the DEKA locus is replaced by the AAAA and DEAA loci. The zero position corresponds to the level of α-carbons in the DEKA locus. Negative coordinates correspond to the extracellular direction. The profile of TMA in the AAAA mutant shows two deep minima. The first one corresponds to the electrostatic interaction of TMA with the external ring of acidic residues. The second minimum is close to the focus of pore helices' axes. Two negatively charged residues in the DEAA mutant eliminate the barrier between the minima and enable the TMA permeation.

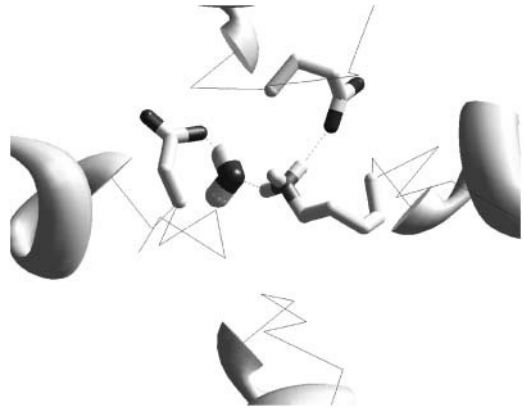

FIGURE 8 A water molecule in the selectivity of the Na^+ channel. Specific interactions in the DEKA locus with the water molecule agree with the model of Lipkind and Fozzard (2000).

chelating a single Ca^{2+} ion (Zhorov and Ananthanarayanan, 1996; Zhorov et al., 2001). To assess the ability of our model to reproduce both concepts, we created the EEEE mutant of the Na^+ channel with two Ca^{2+} ions. Strong electrostatic attractions of two Ca^{2+} ions to four glutamates provided essential stability to both modes of Ca^{2+} chelation even without constraints. Therefore, other arguments and other methods of analysis should be employed to discriminate the two patterns of Ca^{2+} chelation.

DISCUSSION

General properties of the model

In this study, we have built a model of the Na^+ channel P-loops region (Fig. 9) and tested its ability to explain a wide range of experimental data. A critically important feature of our model is its three-dimensional similarity with K^+ channels. In particular, the pore helices are disposed as in MthK and only the selectivity-filter region is rearranged. The rearrangement was made not manually, but via MC-minimization with specific constraints imposed to reproduce the TTX and STX binding. The MC-minimization produced only moderate local rearrangements of the backbones. Subsequent in silico experiments showed that the model explains a wide range of experimental data that were not used at the stage of the model building. In particular, the model predicts quantitative characteristics of the ligand-receptor complexes that correlate with the experimental data. This fact can justify the employment of the model in further studies of Na^+ channels. Furthermore, the methodology of building the Na^+ channel model can be used for modeling homologous regions of other P-loop channels.

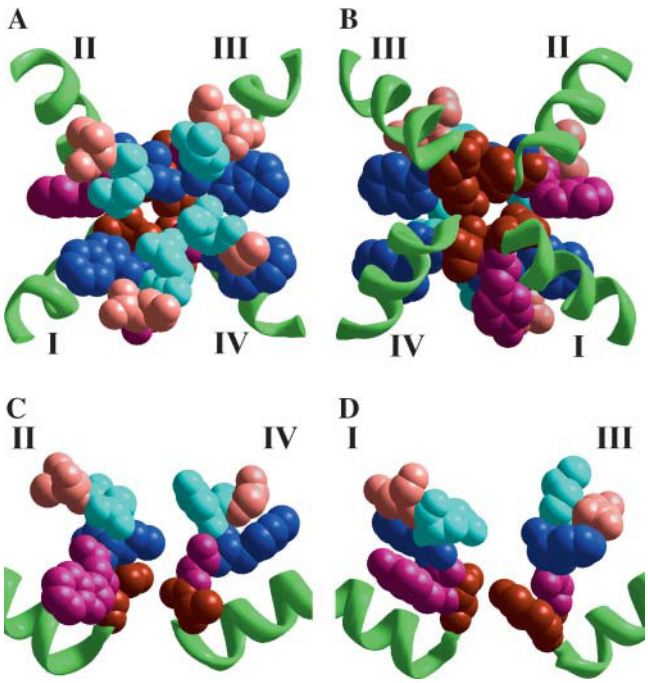

FIGURE 9 The Na^+ channel P-loop region model. The pore helixes are shown as ribbons. The Roman numerals label repeats. The space-filled residues in the DEKA locus are red. The space-filled residues in the downstream positions 1, 2, 3, and 4 from the DEKA locus are colored magenta, blue, cyan, and pink, respectively. (*A*) Extracellular view; (*B*) intracellular view; (*C* and *D*) side views with two nonadjacent repeats.

Our results show that specific pharmacological and electrophysiological properties of the Na^+ channel can be reproduced in the model built via just a local modification of the K^+ channel template in the selectivity-filter region without displacing all P-loops. It seems that the P-loops in Na^+ and K^+ channels have a more similar disposition than was believed. The similar spatial disposition of the pore helices suggests that the inner and outer helices are also arranged similarly in K^+ and Na^+ channels. This justifies the employment of the K^+ channel x-ray structure for homology modeling of the inner pore region of the Na^+ channel. In general, our results suggest that the pore-forming domains in P-loop channels, in addition to sharing the common folding, have conserved three-dimensional structures.

The sequence alignment between K^+ and Na^+ channels is of particular importance because any change in the alignment would dramatically affect the model. K^+ channels are distant from Na^+ and Ca^{2+} channels and the alignment of their sequences is not a trivial task. In this work we used the alignment (Table 1) previously proposed for the modeling of Ca^{2+} channels (Zhorov et al., 2001), which align unambiguously with Na^+ channels. The same alignment was used in a Ca^{2+} channel model in which ligand-sensing residues in the outer, inner, and the pore helices were clustered to form a compact ligand-binding site (Yamaguchi et al., 2003). This alignment can also explain the common positions of ligand-sensing residues in the P-loops of the *Shaker* channel (Rauer and Grissmer, 1999) and Ca^{2+} channel (Yamaguchi et al., 2003). It deserves mentioning that the same alignment explains the involvement of certain P-loop residues in the binding of dihydropyridine ligands to Ca^{2+} channels (Yamaguchi et al., 2003) and guanidinium toxins to the Na^+ channel.

The selectivity filter in the Na^+ channel is essentially wider than in the K^+ channel, whereas the pore helices in both channels have the same position. Although strange at first sight, this feature has a simple explanation. The narrow lumen in the K^+ channel is lined by the backbones of residues, whose side chains are H-bonded to the side chains of other P-loop residues. In contrast, the Na^+ channel selectivity filter is formed by the side chains of residues, whose backbones approach other P-loop residues. The compact packing of the selectivity-filter backbones against the pore helices provides a rather wide lumen in the Na^+ channel model.

When TTX and STX bind to the Na^+ channel, they approach the narrowest part but do not pass it. Therefore, these toxins cannot serve as probes to estimate the size of the lumen. The critical experimental data regarding the lumen size is the permeability of different organic cations (Sun et al.,

1997), which do not pass through the wild-type Na^+ channel, but pass through certain mutants. These data are especially important for our model, in which the P-loops are located closer to the pore axis than in other models. To address this question, we calculated MC-minimized energy profiles for TMA pulled through the Na^+ channel and its mutants. These calculations did not reveal any critical steric obstacles along the permeation pathway.

Molecular pharmacology of Na^+ channel

The energetically optimal complexes of STX and TTX with the Na^+ channel provide a list of specific ligand-receptor contacts, some of which have not been previously resolved. Interestingly, practically all H-bonding groups of TTX and STX found H-bonding partners in the channel. This was achieved by the systematic search of the energetically optimal orientation of the ligands in the selectivity-filter region. Imposing of multiple contacts manually is hardly possible. Our results suggest that the multiple electrostatic and H-bonding interactions are responsible for the high activity of guanidinium toxins. The correlation between the predicted ligand-receptor energy of the TTX analogs and their experimental activity implies that the activity decreases with the number of electrostatic and H-bonding ligand-receptor contacts. The van der Waals and solvation contributions to the ligand-receptor energy do not depend significantly on the structure and orientation of the ligands, because different toxins occupy the same space and have approximately the same contact surface.

In this work we did not attempt to model the entire outer vestibule, since this is a standalone task. Therefore, the current model is not expected to predict the optimal orientation of conotoxins and their binding energy. Nevertheless, some aspects of interaction of certain groups of conotoxins, which are critical for their action at the selectivity-filter region, were analyzed. The results of MCM docking agree with multiple specific contacts found in experiments.

Our model is consistent with the cysteine scanning experiments on the Na^+ channel pore region (Yamagishi et al., 1997; 2001) although our structural interpretation differs from that proposed in the original publications. In particular, the experiments show that the cysteine substitutions of Phe^{1236} and Thr^{1528} at positions immediately preceding the DEKA-locus residues in repeats III and IV, respectively (see Table 1), were accessible for the externally applied reagents (Yamagishi et al., 1997). At first glance, these data conflict with our model, in which Phe^{1236} and Thr^{1528} face the inner pore. Interestingly, however, the above residues face the tunnel formed by the inner helices of repeats III and IV and the pore helix in repeat III (Fig. 10). Residues that affect the action of externally applied Na^+ and Ca^{2+} channel ligands also occur in the same tunnel. In the Ca^{2+} channel model with the pore helices arranged as in the current work, the tunnel is wide enough to accommodate relatively large dihydropyridine molecules (Yamaguchi et al., 2003). Thus, the comparison of the available mutational data with the KcsA x-ray structure suggests that there is a drug-access pathway to the inner pore in Na^+ channels between domains III and IV.

The pore-helix residues at positions −5, −9, and −10 from the DEKA locus (see Table 1) affect the TTX block, but they are not accessible by the external and internal sulfhydryl reagents (Yamaguchi et al., 2000). The selectivity-filter region in our model is tightly packed against the pore helices and almost completely screens the above residues from the lumen. Cysteine substitutions at these positions, on one hand, would not be readily accessible, but on the other hand, they would significantly affect the packing of the selectivity-filter region against the pore helices. This would result in the

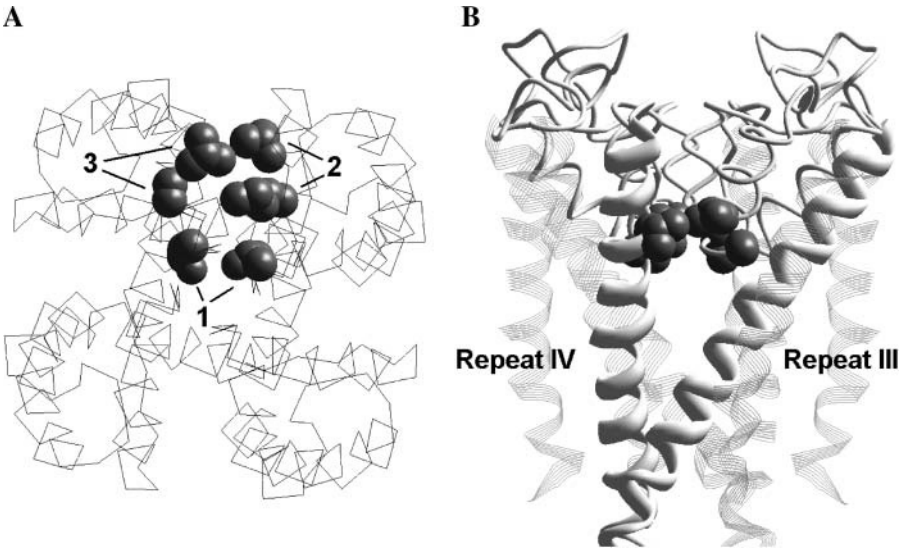

FIGURE 10 Top (*A*) and side (*B*) views of the KcsA crystallographic structure with the access pathway to the pore of P-loop channels highlighted. The solid ribbons in *B* represent the inner helices in repeats III and IV and rods show P-loops. Numbers at *A* denote space-filled KcsA residues in positions where mutations in Na^+ and Ca^{2+} channels affect the action of extracellularly applied ligands. (*1*) Thr^{C75} and Thr^{D75} correspond to the Na^+ channel residues Phe^{1236}Cys and Thr^{1528}Cys that are accessible for extracellular reagents (Yamagishi et al., 1997). (*2*) Val^{D93} and Met^{D96} correspond to the Na^+ channel residues Cys^{1572} and Ile^{1575} that control external access of permanently charged analogs of local anesthetics (Qu et al., 1995; Sunami et al., 2001). (*3*) Val^{C70} and Ala^{C73} correspond to the Ca^{2+} channel Phe^{1112} and Ser^{1115} that control the access of dihydropyridine to the receptor (Yamaguchi et al., 2003).

rearrangement of the side chains that interact with TTX. Since many specific contacts are critical for TTX binding, the rearrangement would reduce the TTX sensitivity of the mutants.

Limitations of our model

Our modeling results agree with a large number of experiments, but it is necessary to emphasize the obvious limitations of our approach. The quality of any model, which is not based on the high-resolution experimental structure, is affected by the imperfect force field and the limited power of the energy optimization methods. Therefore, the energetics alone cannot serve as the criterion of the model correctness. In these circumstances, it is crucial to define constraints that would harmonize the model with obvious experiments even at the expense of increasing the model energy. This limitation makes time-consuming calculations of free energy of ligand-receptor complexes, which aim to predict the absolute activity of ligands, impractical. However, the ligand-receptor energy calculated in this work correlates with the relative activity in a homologous series of ligands. The absolute value of this energy is overestimated because several important components are not included in the energy expression. Thus, the loss of entropy upon the ligand binding and displacement of cations from the acidic residues would compensate the large enthalpy. Experimental data indicate the importance of such effects (Li et al., 2003). The number and location of the counterions in the pore is unknown and the cost for their displacement is difficult to predict.

In the absence of the Na^+ channel x-ray structure, we cannot estimate how correct the predicted torsional angles of the selectivity-filter region may be. But the general disposition of the functional groups in the TTX/STX binding site in our model seems reliable because it explains a wide range of experimental data. Our model cannot predict relative activities of peptide toxins because it does not include extracellular loops. We also did not address the quantitative aspects of selectivity, which would require extensive MD simulations. However, the proposed model could serve as a template for such studies. Coordinates of the model are available (see Supplementary Material).

SUPPLEMENTARY MATERIAL

An online supplement to this article can be found by visiting BJ Online at http://www.biophysj.org.

We thank Iva Bruhova for reading the manuscript and valuable comments. Computations were performed, in part, using the SHARCNET Supercomputer Centre at McMaster University.

This work was supported by a grant to B.S.Z. from the Canadian Institutes of Health Research. B.S.Z. is a recipient of the Canadian Institutes of Health Research Senior Investigator award.

REFERENCES

Aqvist, J., and V. Luzhkov. 2000. Ion permeation mechanism of the potassium channel. *Nature*. 404:881–884.

Backx, P. H., D. T. Yue, J. H. Lawrence, E. Marban, and G. F. Tomaselli. 1992. Molecular localization of an ion-binding site within the pore of mammalian sodium channels. *Science*. 257:248–251.

Becker, S., E. Prusak-Sochaczewski, G. Zamponi, A. G. Beck-Sickinger, R. D. Gordon, and R. J. French. 1992. Action of derivatives of μ-conotoxin $G_{III}A$ on sodium channels. Single amino acid substitutions in the toxin separately affect association and dissociation rates. *Biochemistry*. 31: 8229–8238.

Berneche, S., and B. Roux. 2001. Energetics of ion conduction through the K^+ channel. *Nature*. 414:73–77.

Brooks, C. L., B. M. Pettitt, and M. Karplus. 1985. Structural and energetic effects of truncating long-ranged interactions in ionic polar fluids. *J. Chem. Phys.* 83:5897–5908.

Burnashev, N., A. Villarroel, and B. Sakmann. 1996. Dimensions and ion selectivity of recombinant AMPA and kainate receptor channels and their dependence on Q/R site residues. *J. Physiol.* 496:165–173.

Chahine, M., L. Q. Chen, N. Fotouhi, R. Walsky, D. Fry, V. Santarelli, R. Horn, and R. G. Kallen. 1995. Characterizing the μ-conotoxin binding site on voltage-sensitive sodium channels with toxin analogs and channel mutations. *Receptors Channels*. 3:161–174.

Chahine, M., J. Sirois, P. Marcotte, L. Chen, and R. G. Kallen. 1998. Extrapore residues of the S5–S6 loop of domain 2 of the voltage-gated skeletal muscle sodium channel (rSkM1) contribute to the μ-conotoxin GIIIA binding site. *Biophys. J.* 75:236–246.

Chang, N. S., R. J. French, G. M. Lipkind, H. A. Fozzard, and S. Dudley, Jr. 1998. Predominant interactions between μ-conotoxin Arg-13 and the skeletal muscle Na^+ channel localized by mutant cycle analysis. *Biochemistry*. 37:4407–4419.

Choudhary, G., M. Yotsu-Yamashita, L. Shang, T. Yasumoto, and S. C. Dudley, Jr. 2003. Interactions of the C-11 hydroxyl of tetrodotoxin with the sodium channel outer vestibule. *Biophys. J.* 84:287–294.

Cruz, L. J., W. R. Gray, B. M. Olivera, R. D. Zeikus, L. Kerr, D. Yoshikami, and E. Moczydlowski. 1985. *Conus geographus* toxins that discriminate between neuronal and muscle sodium channels. *J. Biol. Chem.* 260:9280–9288.

Dewar, M. J. S., E. G. Zoebisch, E. F. Healy, and J. J. P. Stewart. 1985. AM1: a new general purpose quantum mechanical model. *J. Am. Chem. Soc.* 107:3902–3909.

Doyle, D. A., J. Morais-Cabral, R. A. Pfuetzner, A. Kuo, J. M. Gulbis, S. L. Cohen, B. T. Chait, and R. MacKinnon. 1998. The structure of the potassium channel: molecular basis of K^+ conduction and selectivity. *Science*. 280:69–77.

Dudley, S. C., Jr., H. Todt, G. Lipkind, and H. A. Fozzard. 1995. A μ-conotoxin-insensitive Na^+ channel mutant: possible localization of a binding site at the outer vestibule. *Biophys. J.* 69:1657–1665.

Dudley, S. C., Jr., N. Chang, J. Hall, G. Lipkind, H. A. Fozzard, and R. J. French. 2000. μ-Conotoxin $G_{III}A$ interactions with the voltage-gated Na^+ channel predict a clockwise arrangement of the domains. *J. Gen. Physiol.* 116:679–690.

Favre, I., E. Moczydlowski, and L. Schild. 1996. On the structural basis for ionic selectivity among Na^+, K^+, and Ca^{2+} in the voltage-gated sodium channel. *Biophys. J.* 71:3110–3125.

Heinemann, S. H., H. Terlau, W. Stuhmer, K. Imoto, and S. Numa. 1992. Calcium channel characteristics conferred on the sodium channel by single mutations. *Nature*. 356:441–443.

Hille, B. 1971. The permeability of the sodium channel to organic cations in myelinated nerve. *J. Gen. Physiol.* 58:599–619.

Hille, B. 1973. Potassium channels in myelinated nerve. Selective permeability to small cations. *J. Gen. Physiol.* 61:669–686.

Huang, C. J., I. Favre, and E. Moczydlowski. 2000. Permeation of large tetra-alkylammonium cations through mutant and wild-type voltage-gated sodium channels as revealed by relief of block at high voltage. *J. Gen. Physiol.* 115:435–454.

Hui, K., G. Lipkind, H. A. Fozzard, and R. J. French. 2002. Electrostatic and steric contributions to block off the skeletal muscle sodium channel by μ-conotoxin. *J. Gen. Physiol.* 119:45–54.

Jiang, Y., A. Lee, J. Chen, M. Cadene, B. T. Chait, and R. MacKinnon. 2002. The open pore conformation of potassium channels. *Nature*. 417:523–526.

Jiang, Y., A. Lee, J. Chen, V. Ruta, M. Cadene, B. T. Chait, and R. MacKinnon. 2003. X-ray structure of a voltage-dependent K^+ channel. *Nature*. 423.

Kao, C. Y., and S. E. Walker. 1982. Active groups of saxitoxin and tetrodotoxin as deduced from actions of saxitoxin analogues on frog muscle and squid axon. *J. Physiol.* 323:619–637.

Kao, C. Y. 1986. Structure-activity relations of tetrodotoxin, saxitoxin, and analogues. *Ann. N. Y. Acad. Sci.* 479:52–67.

Khan, A., L. Romantseva, A. Lam, G. Lipkind, and H. A. Fozzard. 2002. Role of outer ring carboxylates of the rat skeletal muscle sodium channel pore in proton block. *J. Physiol.* 543:71–84.

Kim, M. S., T. Morii, L. X. Sun, K. Imoto, and Y. Mori. 1993. Structural determinants of ion selectivity in brain calcium channel. *FEBS Lett.* 318:145–148.

Kirsch, G. E., M. Alam, and H. A. Hartmann. 1994. Differential effects of sulfhydryl reagents on saxitoxin and tetrodotoxin block of voltage-dependent Na channels. *Biophys. J.* 67:2305–2315.

Kuo, A., J. M. Gulbis, J. F. Antcliff, T. Raham, E. D. Lowe, J. Zimmer, J. Cuthbertson, F. M. Ashcroft, T. Ezaki, and D. A. Doyle. 2003. Crystal structure of the potassium channel $Kir_{Bac1.1}$ in the closed state. *Science*. 300:1922–1926.

Lazaridis, T., and M. Karplus. 1999. Effective energy function for proteins in solution. *Proteins*. 35:133–152.

Li, Z., and H. A. Scheraga. 1987. Monte Carlo-minimization approach to the multiple-minima problem in protein folding. *Proc. Natl. Acad. Sci. USA*. 84:6611–6615.

Li, R. A., R. G. Tsushima, R. G. Kallen, and P. H. Backx. 1997. Pore residues critical for μ-conotoxin binding to rat skeletal muscle Na^+ channels revealed by cysteine mutagenesis. *Biophys. J.* 73:1874–1884.

Li, R. A., K. Hui, R. J. French, K. Sato, C. A. Henrikson, G. F. Tomaselli, and E. Marban. 2003. Dependence of μ-conotoxin block of sodium channels on ionic strength but not on the permeating $[Na^+]$: implications for the distinctive mechanistic interactions between Na^+ and K^+ channel pore-blocking toxins and their molecular targets. *J. Biol. Chem.* 278: 30912–30919.

Li, R. A., I. L. Ennis, R. J. French, S. C. Dudley, Jr., G. F. Tomaselli, and E. Marban. 2001. Clockwise domain arrangement of the sodium channel revealed by μ-conotoxin ($G_{III}A$) docking orientation. *J Biol Chem.* 276: 11072–11077.

Lipkind, G. M., and H. A. Fozzard. 2000. KcsA crystal structure as framework for a molecular model of the Na^+ channel pore. *Biochemistry*. 39:8161–8170.

Lipkind, G. M., and H. A. Fozzard. 2001. Modeling of the outer vestibule and selectivity filter of the L-type Ca^{2+} channel. *Biochemistry*. 40:6786–6794.

McCleskey, E. W., and W. Almers. 1985. The Ca channel in skeletal muscle is a large pore. *Proc. Natl. Acad. Sci. USA*. 82:7149–7153.

Narahashi, T., H. G. Haas, and E. F. Therrien. 1967. Saxitoxin and tetrodotoxin: comparison of nerve blocking mechanism. *Science*. 157: 1441–1442.

Noda, M., H. Suzuki, S. Numa, and W. Stuhmer. 1989. A single point mutation confers tetrodotoxin and saxitoxin insensitivity on the sodium channel II. *FEBS Lett.* 259:213–216.

Ohizumi, Y., S. Minoshima, M. Takahashi, A. Kajiwara, H. Nakamura, and J. Kobayashi. 1986. *Geographutoxin* II, a novel peptide inhibitor of Na channels of skeletal muscles and autonomic nerves. *J. Pharmacol. Exp. Ther.* 239:243–248.

Olivera, B. M., J. Rivier, C. Clark, C. A. Ramilo, G. P. Corpuz, F. C. Abogadie, E. E. Mena, S. R. Woodward, D. R. Hillyard, and L. J. Cruz. 1990. Diversity of *Conus* neuropeptides. *Science*. 249:257–263.

Penzotti, J. L., H. A. Fozzard, G. M. Lipkind, and S. C. Dudley, Jr. 1998. Differences in saxitoxin and tetrodotoxin binding revealed by mutagenesis of the Na^+ channel outer vestibule. *Biophys. J.* 75:2647–2657.

Penzotti, J. L., G. Lipkind, H. A. Fozzard, and S. C. Dudley, Jr. 2001. Specific neosaxitoxin interactions with the Na^+ channel outer vestibule determined by mutant cycle analysis. *Biophys. J.* 80:698–706.

Qu, Y., J. Rogers, T. Tanada, T. Scheuer, and W. A. Catterall. 1995. Molecular determinants of drug access to the receptor site for antiarrhythmic drugs in the cardiac Na^+ channel. *Proc. Natl. Acad. Sci. USA*. 92:11839–11843.

Rauer, H., and S. Grissmer. 1999. The effect of deep pore mutations on the action of phenylalkylamines on the $Kv_{1.3}$ potassium channel. *Br. J. Pharmacol.* 127:1065–1074.

Satin, J., J. W. Kyle, M. Chen, P. Bell, L. L. Cribbs, H. A. Fozzard, and R. B. Rogart. 1992. A mutant of TTX-resistant cardiac sodium channels with TTX-sensitive properties. *Science*. 256:1202–1205.

Sato, K., Y. Ishida, K. Wakamatsu, R. Kato, H. Honda, Y. Ohizumi, H. Nakamura, M. Ohya, J. M. Lancelin, D. Kohda, and F. Inagaki. 1991. Active site of μ-conotoxin GIIIA, a peptide blocker of muscle sodium channels. *J. Biol. Chem.* 266:16989–16991.

Shrivastava, I. H., D. P. Tieleman, P. C. Biggin, and M. S. Sansom. 2002. K^+ versus Na^+ ions in a K channel selectivity filter: a simulation study. *Biophys. J.* 83:633–645.

Stephan, M. M., J. F. Potts, and W. S. Agnew. 1994. The Mu1 skeletal muscle sodium channel: mutation E403Q eliminates sensitivity to tetrodotoxin but not to μ-conotoxins GIIIA and GIIIB. *J. Membr. Biol.* 137:1–8.

Sun, Y. M., I. Favre, L. Schild, and E. Moczydlowski. 1997. On the structural basis for size-selective permeation of organic cations through the voltage-gated sodium channel. Effect of alanine mutations at the DEKA locus on selectivity, inhibition by Ca^{2+} and H^+, and molecular sieving. *J. Gen. Physiol.* 110:693–715.

Sunami, A., I. W. Glaaser, and H. A. Fozzard. 2001. Structural and gating changes of the sodium channel induced by mutation of a residue in the upper third of IVS6, creating an external access path for local anesthetics. *Mol. Pharmacol.* 59:684–691.

Terlau, H., S. H. Heinemann, W. Stuhmer, M. Pusch, F. Conti, K. Imoto, and S. Numa. 1991. Mapping the site of block by tetrodotoxin and saxitoxin of sodium channel II. *FEBS Lett.* 293:93–96.

Tikhonov, D. B., B. S. Zhorov, and L. G. Magazanik. 1999. Intersegment hydrogen bonds as possible structural determinants of the N/Q/R site in glutamate receptors. *Biophys. J.* 77:1914–1926.

Tikhonov, D. B., J. R. Mellor, P. N. Usherwood, and L. G. Magazanik. 2002. Modeling of the pore domain of the GLUR1 channel: homology with K^+ channel and binding of channel blockers. *Biophys. J.* 82:1884–1893.

Tsushima, R. G., R. A. Li, and P. H. Backx. 1997. Altered ionic selectivity of the sodium channel revealed by cysteine mutations within the pore. *J. Gen. Physiol.* 109:463–475.

Wakamatsu, K., D. Kohda, H. Hatanaka, J. M. Lancelin, Y. Ishida, M. Oya, H. Nakamura, F. Inagaki, and K. Sato. 1992. Structure-activity relationships of μ-conotoxin GIIIA: structure determination of active and inactive sodium channel blocker peptides by NMR and simulated annealing calculations. *Biochemistry*. 31:12577–12584.

Weiner, S. J., P. A. Kollman, D. A. Case, U. C. Singh, C. Chio, G. Alagona, S. Profeta, and P. K. Weiner. 1984. A new force field for molecular mechanical simulation of nucleic acids and proteins. *J. Am. Chem. Soc.* 106:765–784.

Yamagishi, T., M. Janecki, E. Marban, and G. F. Tomaselli. 1997. Topology of the P-segments in the sodium channel pore revealed by cysteine mutagenesis. *Biophys. J.* 73:195–204.

Yamagishi, T., R. A. Li, K. Hsu, E. Marban, and G. F. Tomaselli. 2001. Molecular architecture of the voltage-dependent Na channel: functional evidence for α-helices in the pore. *J. Gen. Physiol.* 118:171–182.

Yamaguchi, S., Y. Okamura, T. Nagao, and S. Adachi-Akahane. 2000. Serine residue in the IIIS5–S6 linker of the L-type Ca^{2+} channel α-1C subunit is the critical determinant of the action of dihydropyridine Ca^{2+} channel agonists. *J. Biol. Chem.* 275:41504–41511.

Yamaguchi, S., B. S. Zhorov, K. Yoshioka, T. Nagao, H. Ichijo, and S. Adachi-Akahane. 2003. Key roles of Phe^{1112} and Ser^{1115} in the

pore-forming IIIS_5–S_6 linker of L-type Ca^{2+} channel α-1C subunit ($Cav_{1.2}$) in binding of dihydropyridines and action of Ca^{2+} channel agonists. *Mol. Pharmacol.* 64:235–248.

Yanagawa, Y., T. Abe, and M. Satake. 1987. μ-Conotoxins share a common binding site with tetrodotoxin/saxitoxin on eel electroplax Na channels. *J. Neurosci.* 7:1498–1502.

Yang, J., P. T. Ellinor, W. A. Sather, J. F. Zhang, and R. W. Tsien. 1993. Molecular determinants of Ca^{2+} selectivity and ion permeation in L-type Ca^{2+} channels. *Nature.* 366:158–161.

Yotsu-Yamashita, M., A. Sugimoto, A. Takai, and T. Yasumoto. 1999. Effects of specific modifications of several hydroxyls of tetrodotoxin on its affinity to rat brain membrane. *J. Pharmacol. Exp. Ther.* 289:1688–1696.

Zhorov, B. S. 1981. Vector method for calculating derivatives of energy of atom-atom interactions of complex molecules according to generalized coordinates. *J. Struct. Chem.* 22:4–8.

Zhorov, B. S., and V. S. Ananthanarayanan. 1996. Structural model of a synthetic Ca^{2+} channel with bound Ca^{2+} ions and dihydropyridine ligand. *Biophys. J.* 70:22–37.

Zhorov, B. S., and P. D. Bregestovski. 2000. Chloride channels of glycine and GABA receptors with blockers: Monte Carlo minimization and structure-activity relationships. *Biophys. J.* 78:1786–1803.

Zhorov, B. S., and S. X. Lin. 2000. Monte Carlo-minimized energy profile of estradiol in the ligand-binding tunnel of 17 β-hydroxysteroid dehydrogenase: atomic mechanisms of steroid recognition. *Proteins.* 38:414–427.

Zhorov, B. S., E. V. Folkman, and V. S. Ananthanarayanan. 2001. Homology model of dihydropyridine receptor: implications for L-type Ca^{2+} channel modulation by agonists and antagonists. *Arch. Biochem. Biophys.* 393:22–41.

Zhorov, B. S., and D. B. Tikhonov. 2004. Potassium, sodium, calcium and glutamate-gated channels: pore architecture and ligand action. *J. Neurochem.* 88:782–799.